Reconstruction of tissue scatter characteristics using 3D Ultrasound Tomography

T. Hopp, J. Maul, B. Ebener, M. Zapf, and N.V. Ruiter

Karlsruhe Institute of Technology, Institute for Data Processing and Electronics, Germany

ABSTRACT

Conventional reflectivity imaging with Ultrasound Tomography (USCT) reconstructs qualitative images proportional to the magnitude of the impedance gradient. We propose a method to additionally recover the scatter characteristics for each reconstructed voxel, i.e. whether a reflection is diffuse or specular. This is achieved using a modification of 3D Synthetic Aperture Focusing Technique (SAFT). Our novel approach separates the incoming and outgoing ultrasound intensity in each voxel according to the incident direction and the direction to the receiver. To reduce memory requirements, we propose several strategies for selecting a subset of data or aggregating data to predefined directions. The reconstruction leads to five-dimensional data, from which for each voxel in 3D space, a 2D scatter map can be derived. It can be interpreted as the distribution of energy which has been introduced from a certain direction and which has been reflected into a particular direction. We validated our approach by a simulation based on the Phong reflection model and perform first reconstructions of experimental data. Using the 2D scatter maps it is possible to distinguish specular from diffuse reflections visually. Extracting first-order statistics from the 2D scatter maps for each voxel can be a means to break down the 5D information to 3D for traditional slice-based visualization. The multidimensional data provided by our method may be used in future as a biomarker for diagnosis as e.g. a plain surface of a cyst may reflect the ultrasound differently than a rough surface of a spiculated mass.

Keywords: Ultrasound tomography, reflection imaging, surface characteristics

1. INTRODUCTION

Ultrasound Tomography (USCT) is an emerging non-invasive imaging technology, which currently focuses on early breast cancer detection.[1–3] By surrounding the breast with up to several thousand ultrasound transducers, transmission and reflectivity can be simultaneously acquired. While transmission images represent quantitative sound speed and attenuation properties of tissue, conventional reflection tomography reconstructs qualitative images proportional to the magnitude of the impedance gradient.

At KIT we are developing a full 3D USCT system,[1,4] which arranges the ultrasound transducers in a hemispherical aperture. The aperture has a diameter of approximately 35 cm and is equipped with a total of 2304 transducer, each being able to act as an emitter and receiver. For imaging, one of the transducers emits an approximately spherical wave at a center frequency of 2.6 MHz (bandwidth 3.4 MHz at $-10\,dB$) into the water filled aperture. All other transducers capture the pressure over time, a so-called Amplitude scan (A-Scan).

For reflectivity imaging we apply Synthetic Aperture Focusing Technique (SAFT), which calculates for each voxel the average reflectivity. Scatter characteristics of surfaces are however lost during this reconstruction process: the resulting image only shows that at a certain point in space a reflection of the ultrasound wave occurred, but it is not possible to retrieve whether the surface causing this reflection acts like a point scatterer, a diffuse scatterer or a specular scatterer. This information may be used as a biomarker to discriminate different tissue types as e.g. a plain surface of a cyst may reflect the ultrasound differently than a rough surface of a spiculated mass.

In this work we aim to extend SAFT in order to recover the scatter characteristic at each reconstructed voxel, which is enabled by 3D USCT since it samples the reflected wave at the transducer positions all around the imaged object. Based on our initial work in this field,[5] we here extend, evaluate and validate our approach with simulated data and show first results with experimental data.

Contact: torsten.hopp@kit.edu

2. METHODS

2.1 Reconstruction of surface characteristics

Reflectivity imaging with SAFT sums for each voxel the received amplitudes over all A-scans at a certain time of flight (equation 1). $\vec{x}$ is a voxel in the reflectivity image I, A is the A-scan acquired at a certain emitter i and receiver j and t is the time of flight. To calculate t for a certain emitter-receiver-combination, the Euclidean distance between emitter position $\vec{e}$, the voxel $\vec{x}$, and the receiver position $\vec{r}$ is computed and divided by the sound speed c. c can be approximated by a constant, e.g. based on the water temperature, or by estimating the average sound speed along the traveled path given the reconstructed sound speed image.[6]

$$I(\vec{x}) = \sum_{i,j} A_{i,j}(t) \;\; with \;\; t = \frac{|\vec{e} - \vec{x}| + |\vec{x} - \vec{r}|}{c} \tag{1}$$

While the sum in equation 1 expresses the calculation of the average reflectivity at a certain voxel, our novel approach now separates the incoming and outgoing amplitude in each voxel according to the incident direction $\vec{d}_{in} = (\vec{e} - \vec{x})$ of the emitted wave and the outgoing direction $\vec{d}_{out} = (\vec{r} - \vec{x})$, i.e. instead of a sum over all emitter-receiver combinations as shown in equation 1, we store for each voxel the amplitude for each incident and outgoing direction. Hence equation 4 changes to equation 2

$$I(\vec{x}_{d_i,d_j}) = A_{i,j}(t) \;\; with \;\; t = \frac{|\vec{e} - \vec{x}| + |\vec{x} - \vec{r}|}{c}. \tag{2}$$

Considering the KIT 3D USCT aperture with currently 2304 emitter and 2304 receiver positions this would however require storing 2304 incident $\times$ 2304 outgoing directions per voxel. Typically reconstructed volumes are in the range of 1000^3 voxels leading to approx. 20 Petabyte of memory required per reconstructed volume, which is currently not feasible to keep in memory of reconstruction workstations.

To reduce memory requirements we consider two strategies:

1. on demand reconstruction of small volumes for a particular region of interest (ROI), thereby reducing the number of voxels to be computed and stored,
2. calculation for a subset of N incoming and outgoing directions by either
   (a) reducing the number of emitters and/or receivers or
   (b) aggregating the data which is incident or outgoing from/to approximately the same direction.

For strategy 2b we create per voxel a set of N representative direction vectors ($\vec{d}_k$) with $k \in [1, N]$ (Figure 1). The amplitude is assigned to a $\vec{d}_{k,in}$ and $\vec{d}_{k,out}$ based on a threshold on the angle between $\vec{d}_{in}$ and $\vec{d}_{k,in}$ respectively $\vec{d}_{out}$ and $\vec{d}_{k,out}$. The threshold is chosen as half the angular distance between two neighboring direction vectors.

All strategies lead to a 2D scatter map for each voxel with size $N \times N$. In total the reconstructed volume is thereby five dimensional. The 2D scatter map can be interpreted as the distribution of sound pressure incidenting from a certain direction and which is reflected into a particular direction. To compensate for different magnitudes of reflections from objects with different material, we normalize the scatter maps. Consequently, one would expect more clustered amplitudes to indicate a specular reflection while more distributed amplitudes indicate a diffuse reflection. The scatter maps form the basis for further processing. For example extracting first order statistics from the scatter maps can break down the 5D information to 3D such that conventional slice-based visualization can be applied. Moreover in future a reflectance model can be assumed which forms the basis to estimate reflection coefficients, that can be considered as material constants.

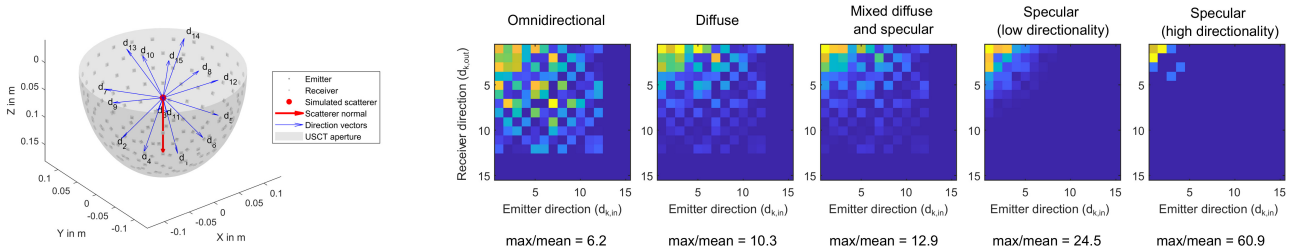

Figure 1: Left: Geometry of USCT aperture (transparent gray) with emitter and receiver positions (gray dots), position of simulated scatterer (red dot) and its normal (red arrow). For reconstruction the directions to emitters and receivers have been discretized to 15 directional vectors (blue arrows). Right: Reconstructed 2D scatter maps for a voxel located at the position of the scatterer. The colors indicate in a blue to yellow colormap the normalized amplitude that has been assigned to a direction vector during reconstruction. Note that some of the predefined directions point out of the 3D USCT's hemispherical aperture leading to zeros in the scatter maps. Different scatter characteristics can be distinguished by the concentration of the amplitude in the scatter maps. The max/mean values represent the maximum amplitude divided by the mean amplitude in each scatter map.

2.2 Data simulation

In order to evaluate our method we simulated data using a ray based approach. We modeled scatterers in the USCT device, which represent one point on a surface, which has a defined normal. The travel time of the reflected ultrasound wave is approximated by the direct path from emitter to scatterer and scatterer to receiver given the sound speed in the surrounding medium. The amplitude A of the received reflection is given according to a simplified Phong reflectance model[7] (equation 3). Here A_0 is the initial amplitude, m_{dif} and m_{spec} are material constants describing the diffuse and specular reflectance of the surface, m_{shine} is the shininess material constant which in our case describes the directionality of the specular reflection. $\vec{x}_s$ is the position of the scatterer and $\vec{p}$ is the direction vector of the perfect reflection given the incident angle and normal of the surface $\vec{n}$.

$$A = A_0 \cdot (m_{dif}((\vec{e} - \vec{x}_s) \cdot \vec{n}) + m_{spec}((\vec{r} - \vec{x}_s) \cdot \vec{p})^{m_{shine}}) \tag{3}$$

The perfect reflection is calculated according to equation 4 by mirroring the incident vector $w = \vec{e} - \vec{x}_s$ on the surface normal vector $\vec{n}$.

$$\vec{p} = \vec{w} - 2 \cdot (\vec{w} \cdot \vec{n}) \cdot \vec{n} \tag{4}$$

3. RESULTS

We simulated scatterers located in USCT aperture with omnidirectional reflection characteristic, diffuse and specular reflection characteristics according to the Phong reflection model with low and high directionality, as well as a mix of diffuse and specular characteristics by setting the according material properties m. The simulated surface normal points towards the bottom of the imaging aperture (Figure 1 left).

First we used strategy 2b to reconstruct volumes and aggregated the data to a set of 15 predefined, uniformly distributed, directions (Figure 1 left). The uniformity of the distribution was optimized following an algorithm of Semechko[8] by an analogy with the minimization of the electro-static potential energy of equally charged particles located on a surface of a unit sphere.

For visualization we show the obtained scatter maps in Figure 1 (right) of the voxel at which the simulated scatterer was located. From the scatter maps omnidirectional scatterers, diffuse scattering objects and specular reflecting objects can be visually distinguished: The more concentrated the amplitudes are to one direction, the more specular the scatterer is reflecting. Note that the last three directions vectors d_{13}, d_{14}, d_{15} got no amplitudes assigned. In these directions no ultrasound transducers are located, such that no A-scans fulfill the threshold criterion to be assigned to them.

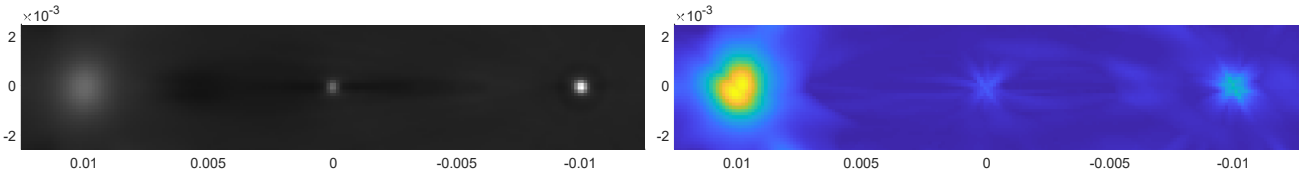

Figure 2: Crossection of a reconstructed volume which includes three scatterers with different characteristic. Left image: conventional SAFT image without respecting scatter characteristics. Right image: for each voxel, the maximum of the 2D scatter map for each voxel is divided by the mean of the 2D scatter map. This ratio is color-coded in a blue to yellow color map. The three scatterers from left to right are reflecting speculary, mixed diffusely and specularly, diffusely.

From the scatter maps we calculated first order statistics to derive a metric expressing the clustering of the amplitudes using the maximum of the scatter map divided by the mean. The value increases gradually from 6.2 for an omnidirectional scatterer to 60.9 for a specular scatterer with high directionality. Using this metric per voxel for an example with three simulated scatterers with different characteristic, it is possible to distinguish specular from diffuse reflectors (Figure 2).

In a second experiment we combined strategy 1 and strategy 2a by reconstructing small sub volumes of $7 \times 7 \times 7$ voxels and selected a subset of 768 emitters and receivers from the full KIT 3D USCT III geometry. Instead of aggregating the amplitudes to predefined directions, we assigned the amplitudes derived from the corresponding A-scans to each emitter and receiver direction, leading to a 2D scatter map of size 768×768 pixels.

We tested this approach with both simulated and experimental data. For the experimental data we imaged a steel sphere with a diameter of 5 *cm*. From the standard SAFT reconstruction we selected two ROIs on the surface of the steel sphere for which we computed the scatter maps, one located at the bottom of the sphere, one located at the side. To ease interpretation and validation of the experimental results we performed simulations based on the Phong model assuming a scatterer located at the position at which the ROIs for the experimental datasets were chosen. The simulated surface normals for those scatterers were defined such that they are approximately the same as in the experimental data, i.e pointing to the bottom of the aperture for the scatterer position located at the bottom of the sphere and pointing to the side of the aperture for the scatterer located at the side of the sphere. Material properties were again varied to simulate diffuse, specular and mixed diffuse and specular characteristics.

The results for the simulations of a scatterer located at the side of the sphere with different characteristics are shown in Figure 3. The x-axis of the scatter maps each represent the receiver numbers sequentially unrolled from the upper ring to the transducer located at the bottom of the hemispherical aperture. The y-axis shows the same order for the emitter positions. The characteristic streaky pattern occurs due to a data selection by limiting the angle between emitter and receiver to 90° in order to image only back reflections for improved contrast and resolution. For the diffuse reflection, the amplitudes are widely distributed to a large range of emitter-receiver-combinations. The more specular the simulated reflection is, the more clustered are the amplitudes to receivers which are located close to the emitter.

Figure 4 presents the resulting scatter maps for a ROI at the bottom (top row) and a ROI at the side (bottom row) of the steel sphere experiment (right column) in comparison to the simulated results assuming a specular reflection with low directionality (left column). The basic pattern in the simulated and experimental scatter maps is comparable, especially for the ROI located at the bottom of the sphere, confirming that the steel sphere reflects the ultrasound wave similar to the specular Phong reflection. For the ROI at the side of the steel sphere the scatter map derived from the simulated data shows a broader distribution, which can be explained by a too optimistic modeling of the transducer opening angle and by neglecting the strong attenuation of the steel sphere in the simulated data. Furthermore differences can be explained by a mismatch in the directionality of the specular reflection in the experimental and simulated data.

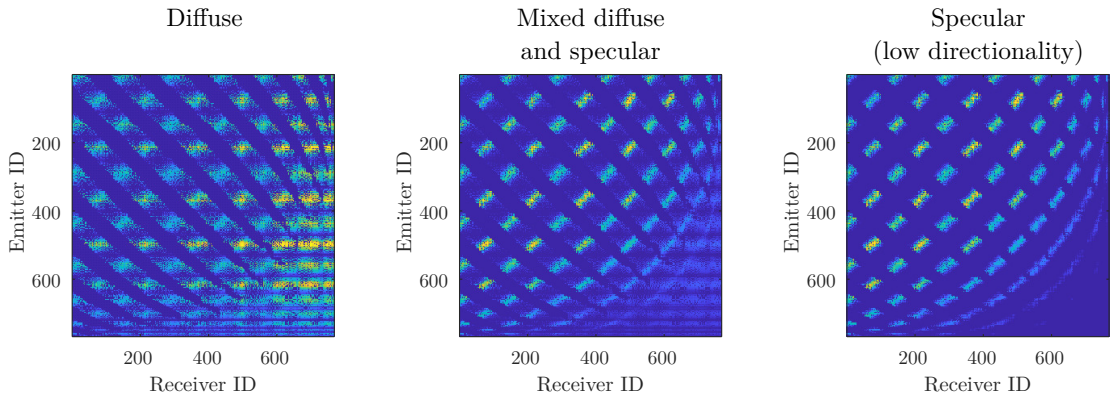

Figure 3: Scatter maps for a voxel showing a reconstructed scatterer with diffuse, mixed diffuse and specular, and specular reflection characteristic using 768 incident and outgoing directions. The scatter maps are normalized and displayed in a blue to yellow colormap.

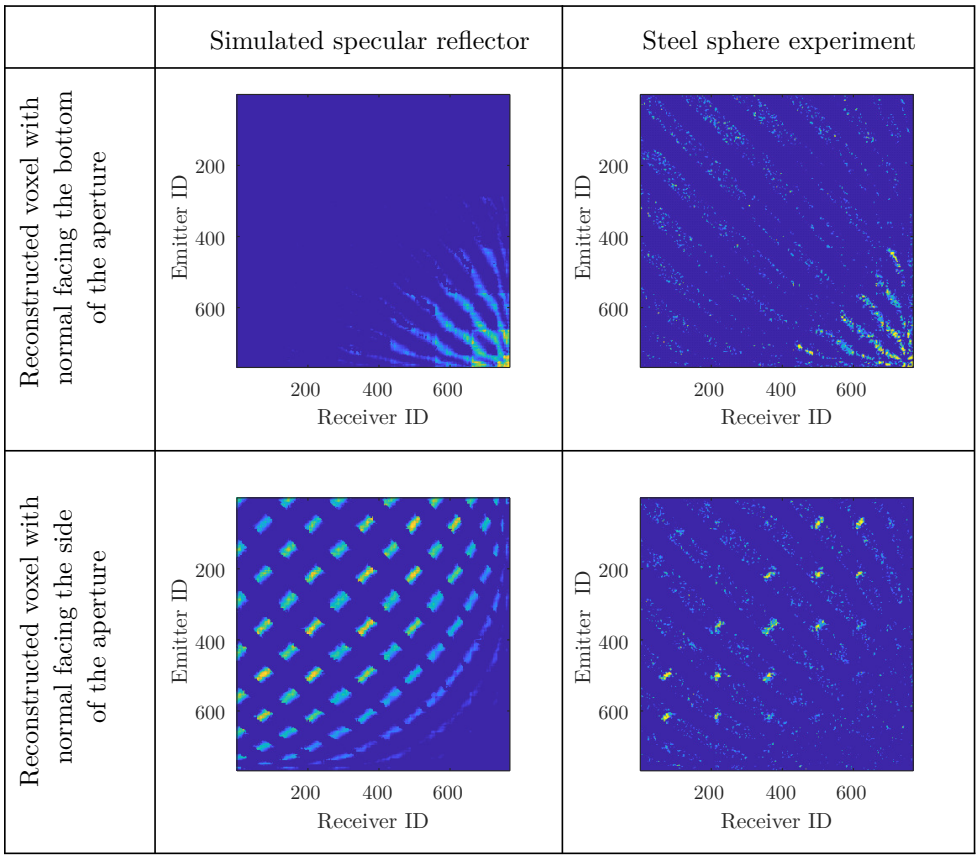

Figure 4: Comparison of scatter maps reconstructed from simulated data assuming a specular reflection with low directionality (left) and from real data experiment with a steel sphere (right). The top row shows the scatter map for a voxel located at the bottom of the steel sphere, the bottom row for a voxel located at the side respectively. The scatter maps are normalized and median filtered and displayed in a blue to yellow colormap.

4. DISCUSSION AND CONCLUSION

In this work we presented a novel approach to assess and quantify the reflectivity characteristics of tissue using 3D Ultrasound Tomography. It extends Synthetic Aperture Focusing Technique by distributing the reflected amplitudes to discrete directions. The multidimensional data may be used in future as a biomarker for diagnosis. The method does not require additional data acquisition, i.e. it uses the once acquired data which is normally used to reconstruct standard reflectivity and transmission images.

Following a prototypical implementation we validated our method with simulated data. For this purpose a simple reflectance model and ray based ultrasound simulation was applied. While this relatively simple simulation model is a limitation of the analysis, it provided us a basic understanding how differently reflecting surfaces may be discriminated. Our validation shows that we can distinguish surface points which reflect more diffuse or more specular given the characteristics of the KIT 3D USCT aperture, even with a very limited number of directions under which the reflectance characteristic is sampled. It has to be noted that the reflectivity characteristics of human tissue are mostly unknown and can only be guessed from their microstructure until now. Hence when establishing the method for breast imaging, the obtained illustrative examples with simulated data can be used as a guide to interpret reconstructions of phantom and patient data in future. First results with experimental data of a steel sphere show similar patterns to simulated data, thereby confirming that with the data acquired by the KIT 3D USCT setup tissue scatter characteristics can be obtained and roughly follow the simple Phong reflectance model.

In a next step we are planning to analyze the method with simulated data of more complex objects and more realistic wave modeling and finally with experimental data of more materials. The novel multidimensional data may serve as a basis for development of advanced multidimensional visualization for doctors or as an input for machine learning approaches to automatically detect and diagnose tumors in future.

REFERENCES

[1] Ruiter, N., Zapf, M., Dapp, R., Hopp, T., Kaiser, W., and Gemmeke, H., "First results of a clinical study with 3d ultrasound computer tomography," in [*2013 IEEE International Ultrasonics Symposium (IUS)*], (2013).

[2] Littrup, P. J., Duric, N., Sak, M., Li, C., Roy, O., Brem, R. F., Larsen, L. H., and Yamashita, M., "Multicenter study of whole breast stiffness imaging by ultrasound tomography (SoftVue) for characterization of breast tissues and masses," *Journal of Clinical Medicine* **10**(23), 5528 (2021).

[3] Malik, B., Iuanow, E., and Klock, J., "An exploratory multi-reader, multi-case study comparing transmission ultrasound to mammography on recall rates and detection rates for breast cancer lesions," *Academic Radiology* **29**, S10–S18 (2022).

[4] Zapf, M., Hopp, T., Gemmeke, H., Angerer, M., Lu, Z., Molchanova, O., Rashvand, N., Blanco, R., Steck, P., Leyrer, B., Tcherniakhovski, D., Bormann, D., Schlote-Holubek, K., and Ruiter, N. V., "Realization of an pseudo-randomly sampled 3d USCT," in [*Medical Imaging 2022: Ultrasonic Imaging and Tomography*], Ruiter, N. V. and Bottenus, N., eds. (2022).

[5] Kretzek, E., Hucker, P., Zapf, M., and Ruiter, N. V., "Evaluation of directional reflectivity characteristics as new modality for 3d ultrasound computer tomography," in [*2015 IEEE International Ultrasonics Symposium (IUS)*], (2015).

[6] Kretzek, E. and Ruiter, N. V., "Gpu based 3d saft reconstruction including phase aberration," in [*Medical Imaging 2014: Ultrasonic Imaging and Tomography*], Bosch, J. G. and Doyley, M. M., eds., SPIE (Mar. 2014).

[7] Phong, B. T., "Illumination for computer generated pictures," *Communications of the ACM* **18**(6), 311–317 (1975).

[8] Semechko, A., "Suite of functions to perform uniform sampling of a sphere." Githbub, https://github.com/AntonSemechko/S2-Sampling-Toolbox (2024).